First Results from the Lyman Alpha Galaxies in the Epoch of Reionization (LAGER) Survey: Cosmological Reionization at $z \sim 7$

Zhen-Ya Zheng[1,2,3], Junxian Wang[4], James Rhoads[5,6], Leopoldo Infante[2], Sangeeta Malhotra[5,6], Weida Hu[4], Alistair R. Walker[7], Linhua Jiang[8], Chunyan Jiang[1,3,9], Pascale Hibon[10], Alicia Gonzalez[5], Xu Kong[4], XianZhong Zheng[11], Gaspar Galaz[2], and L. Felipe Barrientos[2]

[1] CAS Key Laboratory for Research in Galaxies and Cosmology, Shanghai Astronomical Observatory, Shanghai 200030, China; zhengzy@shao.ac.cn
[2] Institute of Astrophysics and Center for Astroengineering, Pontificia Universidad Catolica de Chile, Santiago 7820436, Chile; linfante@astro.puc.cl
[3] Chinese Academy of Sciences South America Center for Astronomy, Santiago 7591245, Chile
[4] CAS Key Laboratory for Research in Galaxies and Cosmology, Department of Astronomy, University of Science and Technology of China, Hefei, Anhui 230026, China; jxw@ustc.edu.cn
[5] School of Earth and Space Exploration, Arizona State University, Tempe, AZ 85287, USA; Sangeeta.Malhotra@asu.edu, James.Rhoads@asu.edu
[6] Astrophysics Science Division, Goddard Space Flight Center, 8800 Greenbelt Road, Greenbelt, MD 20771, USA
[7] Cerro Tololo Inter-American Observatory, Casilla 603, La Serena, Chile
[8] The Kavli Institute for Astronomy and Astrophysics, Peking University, Beijing 100871, China
[9] Núcleo de Astronomía, Facultad de Ingeniería y Ciencias, Universidad Diego Portales, Av. Ejército 441, Santiago, Chile
[10] European Southern Observatory, Alonso de Cordova 3107, Casilla 19001, Santiago, Chile
[11] Purple Mountain Observatory, Chinese Academy of Sciences, Nanjing 210008, China

Abstract

We present the first results from the ongoing Lyman Alpha Galaxies in the Epoch of Reionization (LAGER) project, which is the largest narrowband survey for $z \sim 7$ galaxies to date. Using a specially built narrowband filter NB964 for the superb large-area Dark Energy Camera (DECam) on the NOAO/CTIO 4 m Blanco telescope, LAGER has collected 34 hr NB964 narrowband imaging data in the 3 deg^2 COSMOS field. We have identified 23 Lyα Emitter candidates at $z = 6.9$ in the central 2-deg^2 region, where DECam and public COSMOS multi-band images exist. The resulting luminosity function (LF) can be described as a Schechter function modified by a significant excess at the bright end (four galaxies with $L_{\mathrm{Ly}\alpha} \sim 10^{43.4\pm0.2}$ erg s^{-1}). The number density at $L_{\mathrm{Ly}\alpha} \sim 10^{43.4\pm0.2}$ erg s^{-1} is little changed from $z = 6.6$, while at fainter $L_{\mathrm{Ly}\alpha}$ it is substantially reduced. Overall, we see a fourfold reduction in Lyα luminosity density from $z = 5.7$ to $z = 6.9$. Combined with a more modest evolution of the continuum UV luminosity density, this suggests a factor of ~ 3 suppression of Lyα by radiative transfer through the $z \sim 7$ intergalactic medium (IGM). It indicates an IGM neutral fraction of $x_{\mathrm{H\,I}} \sim 0.4$–$0.6$ (assuming Lyα velocity offsets of 100–200 km s^{-1}). The changing shape of the Lyα LF between $z \lesssim 6.6$ and $z = 6.9$ supports the hypothesis of ionized bubbles in a patchy reionization at $z \sim 7$.

Key words: cosmology: observations – dark ages, reionization, first stars – galaxies: high-redshift – galaxies: luminosity function, mass function

1. Introduction

In the past decade, much progress has been made in narrowing down the epoch of cosmological reionization to be between $z \sim 6$ (Lyα saturation in $z \sim 6$ quasar; Fan et al. 2006) and $z \sim 9$ (Polarization of CMB photons; Planck Collaboration et al. 2016). In between, quasars, gamma-ray bursts (GRBs), and galaxies at $z \gtrsim 6$ are important to constrain the nature of reionization. However, the rarity of high-z quasars (with only one known at $z \gtrsim 7$; Bolton et al. 2011), and of high-z GRBs with rapid follow-up, limit their application as reionization probes. In contrast, hundreds of galaxies at $z \gtrsim 6$ have been reported from ground-based narrowband Lyα line searches (e.g., Ouchi et al. 2010) from space-based broadband Lyman break searches (e.g., Bouwens et al. 2015; Finkelstein et al. 2015) and from newly taken space-based grism spectroscopic surveys (Tilvi et al. 2016; Bagley et al. 2017). Their luminosities, number densities, clustering, and ionizing powers are essential to probe the epoch of reionization (EoR).

Because Lyα photons are resonantly scattered by neutral hydrogen, Lyα emitters (LAEs) provide a sensitive, practical, and powerful tool to determine the epoch, duration, and inhomogeneities of reionization. With a sample of LAEs in EoR, the easiest Lyα reionization test is the luminosity function (LF) test. Rhoads & Malhotra (2001) first applied this test at $z = 5.7$, then at 6.5 (Malhotra & Rhoads 2004; Stern et al. 2005). Subsequent surveys have confirmed and refined the $z = 6.5$–6.6 neutral fraction measurement to $x_{\mathrm{H\,I}} \lesssim 0.3$ (Ouchi et al. 2010; Kashikawa et al. 2011), and have found a significant neutral fraction increase from $z = 6.6$ to $z = 7.3$ (Konno et al. 2014). Other implementations of Lyα reionization tests include the Lyα visibility test (Jensen et al. 2013; Faisst et al. 2014; Schenker et al. 2014), i.e., the Lyα fraction in LBGs in EoR, the volume test (Malhotra & Rhoads 2006; J. Rhoads & S. Malhotra 2017, in preparation), i.e., each Lyα galaxy is taken as evidence for a certain volume of ionized gas, and the clustering test, e.g., the signature of a patchy partially ionized intergalactic medium (IGM) is sought by looking for excess spatial correlations in the Lyα galaxy distribution (Furlanetto et al. 2006; McQuinn et al. 2007; Jensen et al. 2013).

Redshift $z \gtrsim 7$ is the frontier in Lyα and reionization studies. Many searches for LAEs at $z = 6.9$–7.0 (Iye et al. 2006; Ota et al. 2008, 2010; Hibon et al. 2011, 2012), $z = 7.2$–7.3 (Shibuya et al. 2012; Konno et al. 2014), and $z = 7.7$ (Hibon et al. 2010; Tilvi et al. 2010; Krug et al. 2012) have yielded ~two dozen narrowband-selected candidates, but only three of

these have been spectroscopically confirmed so far (Iye et al. 2006; Rhoads et al. 2012; Shibuya et al. 2012). In comparison, hundreds of LAEs have been found at lower redshift at $z = 6.6$ (e.g., Hu et al. 2010; Ouchi et al. 2010; Kashikawa et al. 2011; Matthee et al. 2015), and a large fraction of them have been spectroscopically confirmed (i.e., Kashikawa et al. 2011). The comoving volumes of the searches for $z \gtrsim 7$ LAEs are all less than 6×10^5 cMpc^3, which are more likely to be affected by cosmic variance. In fact, cosmic variance is more important for the observability of LAEs in patchy reionization. Furthermore, some of the surveys with 200 Å wide filters in the far-red inevitably (e.g., Ota et al. 2008, 2010) include one or two weak OH emission lines, limiting their sensitivity. Thus, there is an urgent need for a systematic survey at $z \sim 7$ with sufficient volume and depth to determine if the Lyα line is attenuated due to neutral IGM in a statistically significant way.

In this Letter, we report the discovery of a population of candidate $z \sim 7$ Lyα emitters in the first field (COSMOS) of the Lyman Alpha Galaxies in the Epoch of Reionization (LAGER) survey. With LAGER-COSMOS, we have the largest sample to date of candidate $z \sim 7$ LAEs. In Section 2, we describe the observation and data reduction of LAGER, then introduce the candidates selection method. In Section 3, we present the candidates and their Lyα LF at $z \sim 7$. In Section 4, we discuss the implications of these discoveries for EoR at $z \sim 7$.

2. Survey Description and Data

2.1. LAGER Survey

The LAGER survey is the largest narrowband survey yet for LAEs at $z \gtrsim 7$. It is currently ongoing, using the Dark Energy Camera (DECam, with FOV ~ 3 deg^2) on the NOAO-CTIO 4 m Blanco telescope together with an optimally designed custom narrowband filter, NB964[12] (central wavelength ~ 9642 Å, FWHM ~ 90 Å). LAGER is designed to select more than a hundred $z \sim 7$ LAEs over an area of 12 deg^2 in four fields (8×10^6 cMpc^3). Currently, LAGER has collected 47 hr NB964 narrowband imaging in three fields (CDF-S, COSMOS, and DLS-f5) taken during nine nights in 2015 December, 2016 February, March, and November.

The deepest NB964 imaging is done in COSMOS, where we have obtained 34 hr NB964 exposure in a 3 deg^2 field. The exposure time per NB964 frame is 900 s. Consecutive exposures were dithered by $\sim 100''$ so that chip gaps and bad pixels do not lead to blank areas in the final stacks. We also took ~ 0.5–1 hr z and Y band exposure per field to exclude possible transients. There are deep archival DECam and Subaru broadband images in COSMOS.

2.2. Data Reduction and Analysis

We downloaded the reduced and calibrated DECam resampled images from the NOAO Science Archive, which were processed through the NOAO Community Pipeline (version 3.7.0; Valdes et al. 2014). The individual frames were stacked following the weighting method in Annis et al. (2014) with SWarp (version 2.38.0; Bertin 2010). The seeing of the final stacked LAGER-COSMOS narrowband image is $0''.93$.

The zero-magnitudes of the DECam images were calibrated to the Subaru Suprime-Cam broadband magnitudes of the stars in the public COSMOS/UltraVISTA K_S-selected catalog (Muzzin et al. 2013). We estimated the image depth by measuring the root mean square (rms) of the background in blank places where detected ($>3\sigma$) signals were masked out. In a $2'$ diameter aperture, the 3σ limiting AB magnitudes of the DECam images are $[u, g, r, i, z, Y, NB964]^{3\sigma} = [26.2, 27.4, 26.9, 26.6, 26.1, 24.3, 25.6]$. Deep Subaru Suprime-Cam broadband and narrowband images are available in the central 2-deg^2 area. We downloaded the raw images from the archival server SMOKA (Baba et al. 2002), and produced our own broadband and narrowband stacked images (follow-up work of Jiang et al. 2013). Their 3σ limiting magnitudes within a $2''$ diameter aperture are $[B, g', V, r', i', z', NB711, NB816, NB921]_{3\sigma} \sim [27.9, 27.6, 27.2, 27.4, 27.3, 25.9, 26.0, 26.1, 26.2]$. These Subaru Suprime-Cam images are deeper and have better seeing than the DECam images on average.

We calculated the narrowband completeness via Monte Carlo simulations with the BALROG software (Suchyta et al. 2016). The completeness fraction is defined as the SExtractor recovery percentage of the randomly distributed artificial sources in the NB964 image as a function of narrowband magnitude. For point sources, the narrowband NB964 aperture magnitudes corresponding to the 80%, 50%, and 30% completeness fractions are 24.2, 25.0, and 25.3, respectively. For pseudo LAEs, we choose fake sources similar to those used in Konno et al. (2017), which have a Sérsic profile with the Sérsic index of $n = 1.5$ and the half-light radius of $r_e \sim 0.9$ kpc (0.17 arcsec at $z = 6.9$). The narrowband NB964 aperture magnitudes corresponding to the 80%, 50%, and 30% completeness fractions are 24.3, 24.7, and 25.0 for pesudo LAEs, respectively.

2.3. Selection Criteria for $z \sim 7$ LAEs

Since Subaru broadband images are deeper and have better seeings than those of the DECam broadband images, we only apply selection criteria for $z \sim 7$ LAEs in the central 2-deg^2 area covered by both the Suprime-Cam and the DECam. The selection criteria for $z \sim 7$ LAEs include narrowband NB964 with $\geqslant 5\sigma$ detection (NB964 $\leqslant$ NB964$_{5\sigma}$ = 25.07), narrowband NB964 excess over broadband z (z - NB964 $\geqslant 1.0$),[13] and nondetections in both DECam $ugri$ and Suprime-Cam Bg' $Vr'i'$, N711, N816, N921 bands. We specially exclude broadband detections in the $1''.08$ (4 pixel) diameter aperture to exclude marginal signals in these bands. 156 sources passed the selection criteria, but a large fraction of them are fake sources (bleed trails, diffraction spikes, etc.) after our visual check on NB964 image. With our team's tripartite visual check on both NB964 and broadband images, 27 candidate $z \sim 7$ galaxies are selected. No transient was identified among them using the available broadband images.

---

[12] Please see the filter information at NOAO website: http://www.ctio.noao.edu/noao/content/Properties-N964-filter.

[13] As NB964 lies to the edge of z band transmission curve, very red continuum sources may mimic emission line galaxies. We examine the z–NB versus z–Y plot for bright NB detected sources, and find that red sources with z–Y ~ 1.0 mag have z–NB ~ 0.4 mag, thus such effect is not important.
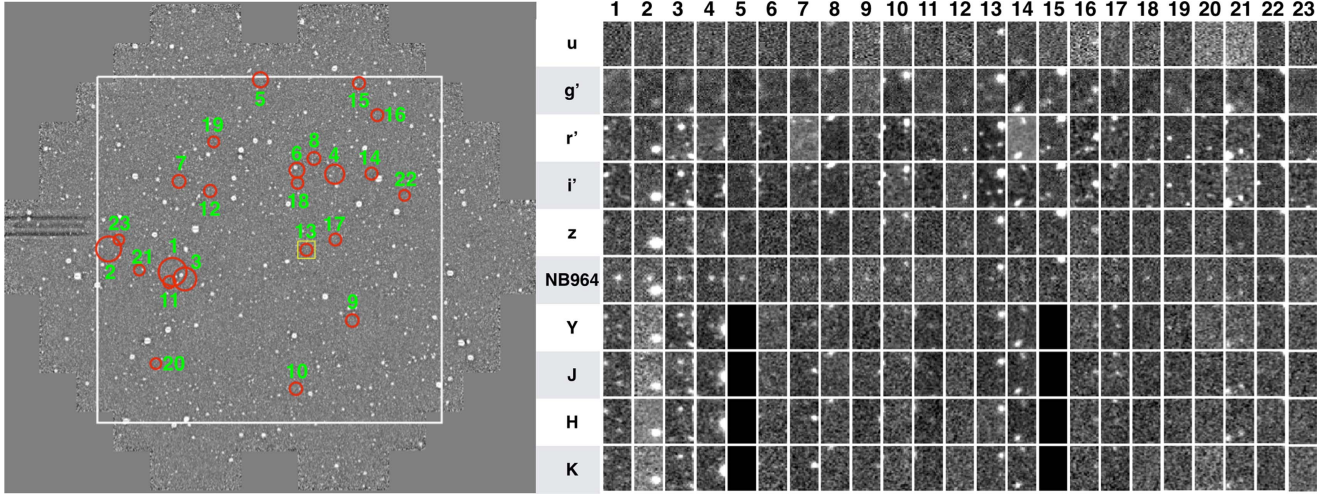
Figure 1. Left: the DECam NB964 COSMOS field showing the uneven distribution of candidate $z \sim 7$ LAEs. The DECam NB964 area is $\sim 3\,\text{deg}^2$, and the overlap region with Subaru Suprime-Cam multi-band images is the central $2\,\text{deg}^2$ area in the white box. We have selected 23 candidate $z \sim 7$ LAEs, which are marked in red circles with aperture sizes scaled to their Lyα line fluxes and normalized to ~ 1 pMpc for the brightest LAE. The only spectroscopically confirmed LAE from previous narrowband survey (Rhoads et al. 2012) in this field is recovered and marked by a yellow box. Right: optical and NIR thumbnail images of the 23 candidate LAEs. We select to display images of DECam u, Suprime-Cam $g'r'i'$, DECam z, DECam NB964, and UltraVISTA (McCracken et al. 2012; DR3) $YJHK$ bands. The stamp size is $10'' \times 5''$.

3. Results

3.1. Candidate LAEs at $z \sim 7$ in LAGER-COSMOS

We estimate the Lyα line fluxes and EWs of the candidates using narrowband and broadband photometry.[14] We further exclude 4 out of the 27 candidates with estimated line EW of <10Å.

In total, 23 candidate $z \sim 7$ LAEs, which have Lyα line fluxes in the range of 0.8–$7.8 \times 10^{-17}\,\text{ergs cm}^{-2}\,\text{s}^{-1}$ and rest-frame equivalent widths $\text{EW}_R \geqslant 10$ Å, are selected. The corresponding observed Lyα line luminosities are 5.4–$43.4 \times 10^{42}\,\text{erg s}^{-1}$. Their positions and their multi-band thumbnail images are plotted in Figure 1.

The four brightest LAEs, with $L(\text{Ly}\alpha) = 19.3$–$43.4 \times 10^{42}\,\text{erg s}^{-1}$, are the most luminous candidate LAEs known at $z \gtrsim 7$, thanks to the large survey volume of LAGER. We have confirmed three of the brightest LAEs at $z \sim 7$ (Hu et al. 2017) with our recent *Magellan*/IMACS spectroscopic follow-up observations.

One of the candidates, J09:59:50.99+02:12:19.1, was previously selected and spectroscopically confirmed as a $z = 6.944$ LAE with *Magellan*/IMACS narrowband imaging and spectroscopy over a much smaller field (Rhoads et al. 2012). It is well recovered with our selection using new DECam narrowband imaging.

3.2. Lyα LF at $z \sim 7$

We use the $V/V_{\max}$ method to calculate the Lyα LF at $z = 6.9$. The formula below is adopted as

$$\Phi(L)dL = \sum_{L_i \in [L - \Delta L/2, L + \Delta L/2]} \frac{1}{V_{\max} f_{\text{comp}}(NB_i)}. \quad (1)$$

---

[14] UltraVISTA Y band (McCracken et al. 2012; DR3) is used to directly estimate the UV continuum of LAGER LAEs. For those without UltraVISTA Y band coverage, we use DECam z band and follow the Appendix of Zheng et al. (2016) to estimate the Lyα line fluxes and EWs. For broadband nondetections, 2σ upper limits are chosen. We assume a flat UV continuum of $f_\nu \propto \nu^0$ and the IGM absorption from Madau (1995) in the above calculations. For candidates with z or Y band detection, such assumption holds within statistical uncertainty.

Table 1
Lyα Luminosity Function at $z \sim 7$ from LAGER-COSMOS Field

$\log_{10}(L_i)$ $(\Delta L = 0.125)$	$N \pm \Delta N^{\text{a}}$ $[L_i \pm \frac{\Delta L}{2}]$	$\langle f_{\text{comp.}} \rangle$	$\log_{10}\Phi(L_i)$ $[(d\log_{10}L)^{-1}\,\text{Mpc}^{-3}]$
42.71	$6^{+3.6}_{-2.4}$	0.21	$-3.74^{+0.20}_{-0.22}$
42.84	$7^{+3.8}_{-2.6}$	0.44	$-4.00^{+0.19}_{-0.20}$
42.96	$4^{+3.2}_{-1.9}$	0.56	$-4.34^{+0.25}_{-0.28}$
43.09	$2^{+2.7}_{-1.3}$	0.80	$-4.80^{+0.37}_{-0.45}$
43.21	<2.6	0.82	<-5.10
43.33	$1^{+2.3}_{-0.8}$	0.85	$-5.13^{+0.52}_{-0.77}$
43.46	$2^{+2.7}_{-1.3}$	0.88	$-4.84^{+0.37}_{-0.45}$
43.59	$1^{+2.3}_{-0.8}$	0.90	$-5.15^{+0.52}_{-0.77}$

Note.
a 1σ Poisson errors from Gehrels (1986).

Here $V_{\max}$ is simply a constant, the maximum survey volume for LAEs ($V_{\max} = 1.26 \times 10^6\,\text{cMpc}^3$ calculated from sky coverage and NB964 central wavelength/FWHM), and $f_{\text{comp}}(NB_i)$ is the detection completeness for sources with narrowband magnitude $m(NB_i)$ interpolated in the narrowband detection completeness for fake LAEs (see Section 2.2).

The Lyα LF of LAEs at $z \sim 7$ in the LAGER-COSMOS field is listed in Table 1, and plotted in Figure 2 together with LAE LFs at $z \sim 5.7$–7.3 from the literature. The LF shows dramatic evolution not only in normalization, but also in the shape.

The relatively fainter end of our LF ($42.65 \leqslant \log_{10}L_{\text{Ly}\alpha} \leqslant 43.25$) at $z \sim 7$ can be fitted with a a single Schechter function in the form of

$$\Phi(L)dL = \Phi^* \left(\frac{L}{L^*}\right)^\alpha \exp\left(-\frac{L}{L^*}\right) d\left(\frac{L}{L^*}\right). \quad (2)$$

Because our survey does not go far below L^*, we fix $\alpha = -2.5$ in our fitting, which is suggested from recent studies on Lyα LFs at $z = 5.7$ and $z = 6.6$ by Konno et al. (2017). Konno et al. (2017) report the largest narrowband surveys to date for LAEs at $z = 5.7$ and $z = 6.6$ taken with Subaru HSC on the
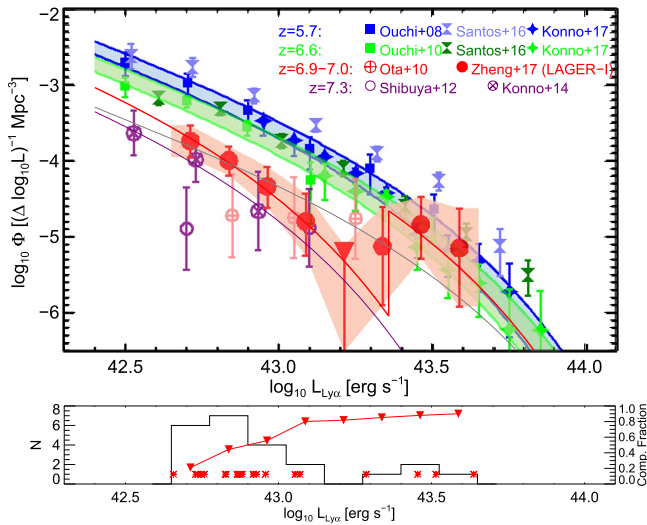
Figure 2. Top: the Lyα LFs of LAE surveys at $z \sim$ [5.7, 6.6, 7, 7.3]. The red filled circles show our results at $z \sim 7$ from the LAGER-COSMOS field. References: Lyα LFs at $z = 5.7$ from Ouchi et al. (2008; blue filled squares), Konno et al. (2017; blue filled stars), and Santos et al. (2016; light-blue filled hourglass), at $z = 6.6$ from Ouchi et al. (2010; green filled squares), Konno et al. (2017; green filled stars), and Santos et al. (2016; dark-green filled hourglass), at $z \sim 7$ from this work (red filled circles) and Ota et al. (2010; pink empty circles with plus), and at $z = 7.3$ from Shibuya et al. (2012; purple empty circles), and Konno et al. (2014; purple empty circles with cross). The colored regions in blue and green show the best Schechter fit with $\pm 1\sigma$ error in L^* at $z \sim 5.7$ and 6.6, respectively, from Konno et al. (2017). The solid and dashed lines in red (gray) show the best Schechter fits at $z \sim 6.9$ with L range $42.65 \leqslant \log_{10} L \leqslant 43.25$ ($42.65 \leqslant \log_{10} L \leqslant 43.65$) (see Table 2). A truncated Schechter function is also plotted (red solid line, see the text for details) to measure the bright-end LF bump. The purple line shows the best Schechter fit at $z \sim 7.3$ from Konno et al. (2014). All these Schechter fits have a fixed faint-end slope of $\alpha = -2.5$. Bottom: the histogram of Lyα luminosities of LAGER LAEs. The average completeness fraction for our LAEs interpolated from Section 2.2 is also plotted as a red solid line with red triangles.

14–21 deg^2 sky, and their best-fit Schechter function analyses also include the smaller but much deeper narrowband surveys taken with Subaru Suprime-Cam (Ouchi et al. 2008, 2010) at the corresponding redshifts. Considering that the Lyα LFs by Konno et al. (2017) are derived from the largest LAE samples at $z = 5.7$ and $z = 6.6$ with the widest luminosity range, and we have used consistent selection and analysis methods, we choose their Lyα LFs for comparison in the following sections. At $z > 7$, we choose the Lyα LF at $z = 7.3$ by Konno et al. (2014) for comparison. The best-fit Schechter function parameters of these LFs are listed in Table 2 and plotted in the upper panel of Figure 3. We find a large drop in Φ of Lyα LF, compared with that at $z = 5.7$ and $z = 6.6$. In the relatively fainter end, our Lyα LF at $z \sim 7$ is in agreement within the 1σ measurement uncertainties of that at $z = 7.3$.

More strikingly, we see a clear bump, i.e., significant excess to the Schechter function in the bright end of our $z \sim 7$ LF ($\log_{10} L_{\text{Ly}\alpha} \gtrsim 43.25$). It demonstrates that, while the space density of faint LAEs drops tremendously from $z = 5.7$ and 6.6 to $z = 6.9$, the luminous LAEs show no significant change. Similarly but much less prominently, the LF evolution between $z = 5.7$ and $z = 6.6$ may also be differential, with a significant decline at the faint end, but not clear evolution at the bright end (Matthee et al. 2015; Santos et al. 2016; Konno et al. 2017). In Figure 2 we also plot a scaled-down and truncated version (red solid line at high luminosity end) of Lyα LF at $z = 5.7$ from

Konno et al. (2017), normalized by the UV luminosity density evolution[15] between $z = 5.7$ and $z = 6.9$, which appears consistent with our LF at the bright end within statistical uncertainties.

4. Discussion

4.1. The Evolution of Lyα LF in EoR

Cosmological reionization was well under way by $z \sim 9$ (Planck Collaboration et al. 2016) and ended by $z \sim 6$ (Fan et al. 2006). Lyα galaxies at $z \gtrsim 6$, e.g., from LAE surveys at $z = 5.7$ (Ouchi et al. 2008; Santos et al. 2016; Konno et al. 2017), at $z = 6.6$ (Ouchi et al. 2010; Matthee et al. 2015; Konno et al. 2017), at $z = 6.9$ (our LAGER-COSMOS sample in this work and Ota et al. 2017), and at $z = 7.3$ (Konno et al. 2014), are unique samples useful to probe both galaxy evolution and reionization.

In this work, we detect for the first time a significant bump at the bright end of Lyα LF at $z \gtrsim 7$. Previous surveys for LAEs at $z \gtrsim 7$ failed to reveal a bump as they covered much smaller volumes.

The existence of such a bright-end bump is consistent with the scenario proposed by Haiman & Cen (2005), that bright LAEs are less attenuated by a neutral IGM than faint LAEs, as the larger Strömgren sphere surrounding luminous LAEs alleviates the neutral IGM absorption (also see Santos et al. 2016; Konno et al. 2017). Therefore, the evolution in the bright end of the LF better reflects the intrinsic evolution of LAEs, while the faint end is controlled by the evolution of both galaxies and the IGM.

The bottom panel of Figure 3 shows the evolution of luminosity densities both for Lyα and UV photons. Compared to LBGs (yellow shaded region), an accelerated evolution of LAE Lyα densities from $z = 6.6$ (green diamonds) to $z = 7.3$ (purple cross), as reported by Konno et al. (2014), is clearly seen in Figure 3. Seeing that UV photons detected in LBGs are insensitive to the neutral hydrogen in EoR, Konno et al. (2014) concluded that such rapid evolution in LAE LFs can be attributed to a large neutral IGM fraction at $z \sim 7.3$. Our LAGER survey shows rapid evolution from $z = 6.6$ to 6.9, and a smaller difference between $z = 6.9$ and 7.3 (see Figure 3). It is possible that the evolution in the neutral fraction accelerated after $z = 6.9$, though a smooth, monotonic neutral fraction evolution at $6.6 \leqslant z \leqslant 7.3$ also fits the LAGER results and the measurements of Konno et al. (2014) within their uncertainties. Note that the cosmic time from $z \sim 6.6$ to 6.9 and from $z \sim 6.9$ to 7.3 are approximately equal, which is about 50 Myr.

Furthermore, compared to the evolution of Lyα densities $\rho_{\text{Ly}\alpha}$ between redshifts of 5.7 and 6.9, the evolution in the bright end only $\rho_{\text{Ly}\alpha}^{\text{Bright}}$ follows a much smoother trend, somehow similar to that of the UV densities of LBGs (bottom panel of Figure 3). This demonstrates that either the intrinsic LAE LF evolves moderately between $z = 5.7$ and 6.9, or that IGM attenuation plays a role even at the highest luminosity bin. Consequently, the dramatic and rapid evolution between $z = 6.6$ and 6.9 in the faint end can be mainly attributed to the change of neutral IGM fraction. This evolution trend is in agreement with the Lyα fraction test which shows the fraction of LBGs with visible Lyα lines drops significantly at $z \gtrsim 7$ (e.g., Schenker et al. 2014).

Table 2
Best-fit Schechter Parameters and Lyα Luminosity Densities at $z \sim 5.7$, 6.6, 6.9, and 7.3

z (1)	Area (2) deg²	Volume (3) [cMpc³]	L Fitted Range (4)	$\log_{10}[L^*_{\mathrm{Ly}\alpha}]$ (5) [erg s⁻¹]	$\log_{10}[\Phi^*]$ (6) [Mpc⁻³]	$\log_{10}[\rho_{\mathrm{Ly}\alpha}]$[a] (7) [erg s⁻¹ Mpc⁻³]	$\log_{10}[\rho^{\mathrm{Bleft}}_{\mathrm{Ly}\alpha}]$[b] (8) [erg s⁻¹ Mpc⁻³]	Reference (9)
				Two free parameters $[L^*_{\mathrm{Ly}\alpha}, \Phi]^*$ with fixed $\alpha = -2.5$				
5.7	13.8	1.16×10^7	42.4–44.0	43.24 ± 0.05	$-4.09^{+0.13}_{-0.11}$	39.54 ± 0.01	38.24	Ouchi et al. (2008) + Konno et al. (2017)
6.6	21.2	1.91×10^7	42.4–44.0	$43.25^{+0.06}_{-0.05}$	-4.32 ± 0.13	39.33 ± 0.02	38.05	Ouchi et al. (2010) + Konno et al. (2017)
6.9	2.0	1.26×10^6	42.65–43.25	$42.77^{+0.32}_{-0.16}$	$-3.77^{+0.54}_{-0.76}$	[c]$38.92^{+0.03}_{-0.04}$	[c]37.90	This study
			42.65–43.65	$43.74^{+0.55}_{-0.38}$	$-5.76^{+0.72}_{-0.81}$	38.77 ± 0.05	37.82	This study
7.3	0.45	2.5×10^5	42.4–43.0	$42.77^{+1.23}_{-0.34}$	$-4.09^{+1.09}_{-1.91}$	$38.55^{+0.08}_{-0.07}$	[d]...	Konno et al. (2014)

Notes. The best-fit parameters in column 5 and column 6 are derived by fitting the Schechter function with fixed $\alpha = -2.5$ on the Lyα LFs listed in column 9 with the χ^2-statistics. The errors in columns 5–7 are estimated from their 1σ confidence contours (e.g., Coe 2009) shown in the top panel of Figure 3.
[a] Lyα luminosity densities integrated over the best-fit Schechter functions at $42.4 < \log_{10}L_{\mathrm{Ly}\alpha} < 44.0$ (column 7). Note the errors of Lyα luminosity densities are likely underestimated because we do not consider the uncertainties of the faint-end slope in that calculation.
[b] Lyα luminosity densities integrated at the bright end ($43.3 < \log_{10}L_{\mathrm{Ly}\alpha} < 43.7$; column 8).
[c] The Lyα luminosity densities in this row are calculated by integrating the truncated Schechter function plotted as the red solid curve in Figure 2 and discussed in Section 3.2. We use the Lyα density in column 7 of this row to estimate the neutral IGM fraction at $z \sim 7$ in Section 4.2.
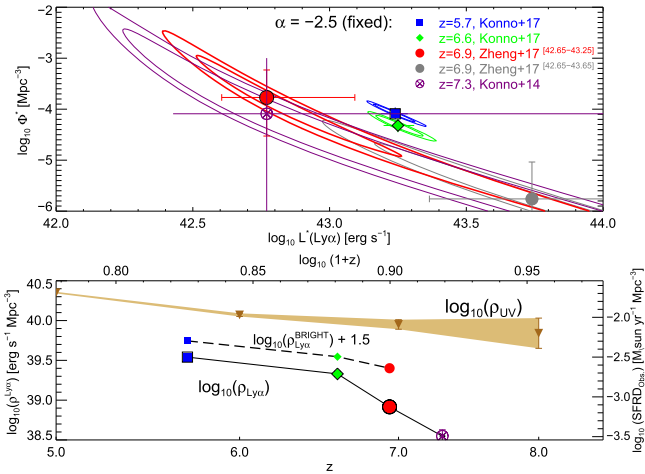[d] The survey for $z = 7.3$ LAEs does not have large enough volume to cover the bright end.

Figure 3. Top: the evolution of best-fit schechter parameters $L^*_{\mathrm{Ly}\alpha}$ and $\Phi^*_{\mathrm{Ly}\alpha}$ of Lyα LFs at $z = [5.7, 6.6, 6.9, 7.3]$ with 1 and 2σ error contours. Bottom: evolution of Lyα and UV luminosity densities at $z \gtrsim 6$. We plot the Lyα luminosity densities integrated over the best-fit Schechter functions ($42.4 < \log_{10}L_{\mathrm{Ly}\alpha} < 44.0$) and at the bright end ($43.3 < \log_{10}L_{\mathrm{Ly}\alpha} < 43.7$). Please see Table 2 for the values. Note that the bright luminosity density is scaled up by 1.5 dex. The yellow shaded region represents the UV luminosity densities for $L_{\mathrm{UV}} > 0.03\, L^*_{\mathrm{UV}}$ given by Finkelstein et al. (2015) at $z \sim 5.0$, 6.0, 7.0, and 8.0. The symbols are the same as for those in Figure 2.

4.2. Neutral IGM Fraction at $z \sim 7$ with LAGER

Following Ouchi et al. (2010) and Konno et al. (2014), we compare the Lyα luminosity densities at $z = 6.9$ (in EoR) and at $z = 5.7$ (when reionization is completed) to estimate the effective IGM transmission factor $T^{\mathrm{IGM}}_{\mathrm{Ly}\alpha,z}$. Assuming the stellar population, interstellar medium (ISM), and dust are similar at $z = 6.9$ and $z = 5.7$, we obtain that

$$T'_{z=6.9} = \frac{T^{\mathrm{IGM}}_{\mathrm{Ly}\alpha,z=6.9}}{T^{\mathrm{IGM}}_{\mathrm{Ly}\alpha,z=5.7}} = \frac{\rho^{Ly\alpha}_{z=6.9}/\rho^{Ly\alpha}_{z=5.7}}{\rho^{\mathrm{UV}}_{z=6.9}/\rho^{\mathrm{UV}}_{z=5.7}}. \quad (3)$$

Here ρ^{UV} and $\rho^{\mathrm{Ly}\alpha}$ are UV and Lyα luminosity densities, respectively. The ratio of UV luminosity densities

$\rho^{\mathrm{UV}}_{z=6.9}/\rho^{\mathrm{UV}}_{z=5.7} = 0.63 \pm 0.09$ is obtained from Finkelstein et al. (2015). We obtain the ratio of observed Lyα luminosity densities (column 7 in Table 2) $\rho^{Ly\alpha}_{z=6.9}/\rho^{Ly\alpha}_{z=5.7} = 0.24 \pm 0.03$. Thus, we estimate $T'_{z=6.9} = 0.38 \pm 0.07$[16] (cf., $T'_{z=7.3} = 0.29$ from Konno et al. 2014 and $T'_{z=6.6} = 0.70 \pm 0.15$ from Konno et al. 2017).

Converting the Lyα emission line transmission factor to neutral IGM fraction $x_{\mathrm{H\,I}}$ is model dependent (e.g., Santos 2004; Dijkstra et al. 2007; McQuinn et al. 2007). An important factor is the shift of the Lyα line with respect to the systemic velocity, which is widely observed and may be explained by Lyα radiative transfer in a galactic wind or outflow. The Lyα velocity shift measurements of $z \sim 6$–7 galaxies are very limited and are mostly around 100–200 km s⁻¹ (Stark et al. 2015, 2017; Pentericci et al. 2016; but see the two UV luminous galaxies with 400–500 km s⁻¹ reported by Willott et al. 2015). With the analytic model of Santos (2004), assuming a Lyα velocity shift of 0 and 360 km s⁻¹, the value of $T'_{z=6.9} = 0.38$ corresponds to $x_{\mathrm{H\,I}} \sim 0.0$ and 0.6, respectively.

By comparing our observed Lyα LF at $z = 6.9$ to that predicted with the radiative transfer simulations by McQuinn et al. (2007; their Figure 4), we obtain $x_{\mathrm{H\,I}} \sim 0.40$–0.60 at $z = 6.9$. Similar results are obtained in the analytic studies considering ionization bubbles (Furlanetto et al. 2006; Dijkstra et al. 2007). We should note that these studies predicted a suppression of the LF that is rather uniform across a wide range of luminosities (e.g., Section 4 of McQuinn et al. 2007). This suggests that the true distribution of ionized region sizes may differ appreciably from those used in the literature (Furlanetto et al. 2006; Dijkstra et al. 2007; McQuinn et al. 2007). We conclude that the neutral hydrogen fraction is $x_{\mathrm{H\,I}} \sim 0.4$–0.6 at $z = 6.9$, where both the uncertainties in the IGM transmission factor calculation and the theoretical model predictions are considered. The LBG Lyα fraction test by Schenker et al. (2014) yields a similar neutral hydrogen fraction

---

[16] Note that the error of $T'_{z=6.9}$ is likely underestimated, as we ignore the uncertainties from the faint-end slope of the Lyα LFs.

($x_{H\,I} = 0.39^{+0.08}_{-0.09}$) at $z \sim 7$. Note that smaller $x_{H\,I} = 0.3 \pm 0.2$ at $z = 6.6$ is obtained by Konno et al. (2017) with Subaru HSC and Suprime-Cam surveys.

4.3. Ionized Bubbles at $z \sim 7$

The bump at the bright end of the Lyα LF is an indicator of large enough (>1 pMpc radius) ionized bubbles, where the Hubble flow can bring Lyα photons out of resonance, thus leading to a different evolution of Lyα LF at the bright end and the faint end. The uneven distribution of these LAEs may indicate ionized bubbles in a patchy reionization at $z \sim 7$. Larger LAGER samples in future will more definitely establish whether the degree of clustering in Figure 1 requires patchy reionization.

The origin of the ionized bubbles could be extrinsic, intrinsic, or both. From Malhotra & Rhoads (2006), which gave the proper radius of a Strömgren sphere and the Gunn–Peterson effect optical depth of a LAE with outflow velocity ΔV in EoR, we know that even the brightest LAE can not produce a large enough ionized bubble to effectively reduce the optical depth to $\tau \sim 1$. We thus would expect extrinsic contribution from additional satellite galaxies associated with the luminous LAEs. From Figure 1, we see such fainter nearby sources (e.g., the projected separations between LAE-1, 3, and 11 are $\lesssim 3.4$ arcmin, which corresponds to 1 pMpc at $z = 6.93$). Further, deeper narrowband imaging would enable us to probe the bubbles by detecting more fainter galaxies associated with the luminous LAEs.

The intrinsic explanation is that these luminous LAEs may be physically unusual objects, perhaps of a type not commonly found at lower redshift. For example, they could represent an AGN population that dominates over the ordinary star-forming galaxies at $\lg_{10}L_{Ly\alpha} > 43.3$ (e.g., Matsuoka et al. 2016). Alternatively, they could be star-forming galaxies where metallicities and/or dust abundances are low enough to enable considerably larger Lyα production or escape than is commonly seen at $z < 6$ (e.g., Stark et al. 2015, 2017; Mainali et al. 2017). At $z \sim 7$, Bowler et al. (2014) find an excess of luminous LBGs where there should be an exponential cutoff at the bright end of their UV LFs. NIR and FIR spectroscopic follow-up of these luminous LBGs show very large Lyα velocity offsets (>300 km s^{-1}; Willott et al. 2015; Stark et al. 2017), which are significantly larger than the predicted velocity offsets for galaxies in EoR by Choudhury et al. (2015). Besides that, unusually strong carbon lines reported in two other LBGs at $z \sim 7$ (C IV λ1548 Å in A1703-zd6 at $z = 7.045$ and C III] 1909 Å in EGS-zs8-1 at $z = 7.73$) indicate unusual harder and more intense UV radiation than that of $z \sim 3$ LBGs (Stark et al. 2015, 2017). In addition, a strong He II line has been reported in the brightest Lyα emitter at $z = 6.6$ (CR7), suggesting that it could be powered by either Pop. III stars (Sobral et al. 2015) or perhaps powered by accretion onto a direct collapse black hole (Pallottini et al. 2015).

Future deeper NB964 imaging and IR (NIR and/or FIR) spectroscopic observation will help us to determine the nature of these luminous LAEs, and probe the ionized bubbles in a patchy reionization at $z \sim 7$.

5. Conclusion

In this Letter, we report the first results of our LAGER project, the discovery of 23 (22 new) candidate LAEs at $z \sim 7$. This is the largest sample to date of candidate LAEs at $z \gtrsim 7$. Furthermore, thanks to the large survey volume of LAGER, we find four most luminous candidate LAEs at $z \sim 7$ with $L(Ly\alpha) = 19$–43×10^{42} erg s^{-1}. Compared to previous Lyα LFs at $z \gtrsim 6$, the Lyα LF of LAGER LAEs at $z \sim 7$ shows different evolution at the faint end and at the bright end, which indicates a large neutral hydrogen fraction of $x_{H\,I} \sim 0.4$–0.6 and the existence of ionized bubbles at $z \sim 7$. Our findings support the patchy reionization scenario at $z \sim 7$.

References

Annis, J., Soares-Santos, M., Strauss, M. A., et al. 2014, ApJ, 794, 120

Baba, H., et al. 2002, in ASP Conf. Ser. 281, Astronomical Data Analysis Software and Systems XI, ed. D. A. Bohlender, D. Durand, & T. H. Handley (San Francisco, CA: ASP), 298

Bagley, M. B., Scarlata, C., Henry, A., et al. 2017, ApJ, 837, 11

Bertin, E. 2010, SWarp: Resampling and Co-adding FITS Images Together, Astrophysics Source Code Library, ascl:1010.068

Bolton, J. S., Haehnelt, M. G., Warren, S. J., et al. 2011, MNRAS, 416, L70

Bouwens, R. J., Illingworth, G. D., Oesch, P. A., et al. 2015, ApJ, 803, 34

Bowler, R. A. A., Dunlop, J. S., McLure, R. J., et al. 2014, MNRAS, 440, 2810

Choudhury, T. R., Puchwein, E., Haehnelt, M. G., et al. 2015, MNRAS, 452, 261

Coe, D. 2009, arXiv:0906.4123

Dijkstra, M., Wyithe, J. S. B., & Haiman, Z. 2007, MNRAS, 379, 253

Faisst, A. L., Capak, P., Carollo, C. M., et al. 2014, ApJ, 788, 87

Fan, X., Strauss, M. A., Becker, R. H., et al. 2006, AJ, 132, 117

Finkelstein, S. L., Ryan, R. E., Jr., Papovich, C., et al. 2015, ApJ, 810, 71

Furlanetto, S. R., Zaldarriaga, M., & Hernquist, L. 2006, MNRAS, 365, 1012

Gehrels, N. 1986, ApJ, 303, 336

Haiman, Z., & Cen, R. 2005, ApJ, 623, 627

Hibon, P., Cuby, J.-G., Willis, J., et al. 2010, A&A, 515, A97

Hibon, P., Kashikawa, N., Willott, C., et al. 2012, ApJ, 744, 89

Hibon, P., Malhotra, S., Rhoads, J., & Willott, C. 2011, ApJ, 741, 101

Hu, E. M., Cowie, L. L., Barger, A. J., et al. 2010, ApJ, 725, 394

Hu, W., Wang, J. X., Zheng, Z. Y., et al. 2017, ApJL, submitted (arXiv:1706.03586)

Iye, M., Ota, K., Kashikawa, N., et al. 2006, Natur, 443, 186

Jensen, H., Laursen, P., Mellema, G., et al. 2013, MNRAS, 428, 1366

Jiang, L. H., Egami, E., Mechtley, M., et al. 2013, ApJ, 772, 99

Kashikawa, N., Shimasaku, K., Matsuda, Y., et al. 2011, ApJ, 734, 119

Konno, A., Ouchi, M., Ono, Y., et al. 2014, ApJ, 797, 16

Konno, A., Ouchi, M., Shibuya, T., et al. 2017, PASJ, submitted (arXiv:1705.01222)

Krug, H. B., Veilleux, S., Tilvi, V., et al. 2012, ApJ, 745, 122

Madau, P. 1995, ApJ, 441, 18

Mainali, R., Kollmeier, J. A., Stark, D. P., et al. 2017, ApJL, 836, L14

Malhotra, S., & Rhoads, J. E. 2004, ApJL, 617, L5

Malhotra, S., & Rhoads, J. E. 2006, ApJL, 647, L95

Matsuoka, Y., Onoue, M., Kashikawa, N., et al. 2016, ApJ, 828, 26

Matthee, J., Sobral, D., Santos, S., et al. 2015, MNRAS, 451, 400

McCracken, H. J., Milvang-Jensen, B., Dunlop, J., et al. 2012, A&A, 544, A156

McQuinn, M., Hernquist, L., Zaldarriaga, M., & Dutta, S. 2007, MNRAS, 381, 75

Muzzin, A., Marchesini, D., Stefanon, M., et al. 2013, ApJS, 206, 8

Ota, K., Iye, M., Kashikawa, N., et al. 2008, ApJ, 677, 12

Ota, K., Iye, M., Kashikawa, N., et al. 2010, ApJ, 722, 803

Ota, K., Iye, M., Kashikawa, N., et al. 2017, ApJ, in press (arXiv:1703.02501)

Ouchi, M., Shimasaku, K., Akiyama, M., et al. 2008, ApJS, 176, 301

Ouchi, M., Shimasaku, K., Furusawa, H., et al. 2010, ApJ, 723, 869

Pallottini, A., Ferrara, A., Pacucci, F., et al. 2015, MNRAS, 453, 2465

Pentericci, L., Carniani, S., Castellano, M., et al. 2016, ApJL, 829, 11

Planck Collaboration, Ade, P. A. R., Aghanim, N., et al. 2016, A&A, 594, A13

Rhoads, J. E., Hibon, P., Malhotra, S., et al. 2012, ApJL, 752, L28

Rhoads, J. E., & Malhotra, S. 2001, ApJL, 563, L5

Santos, M. R. 2004, MNRAS, 349, 1137

Santos, S., Sobral, D., & Matthee, J. 2016, MNRAS, 463, 1678

Schenker, M. A., Ellis, R. S., Konidaris, N. P., & Stark, D. P. 2014, ApJ, 795, 20

Shibuya, T., Kashikawa, N., Ota, K., et al. 2012, ApJ, 752, 114

Sobral, D., Matthee, J., Darvish, B., et al. 2015, ApJ, 808, 139

Stark, D. P., Ellis, R. S., Charlot, S., et al. 2017, MNRAS, 464, 469

Stark, D. P., Richard, J., Charlot, S., et al. 2015, MNRAS, 450, 1846

Stern, D., Yost, S. A., Eckart, M. E., et al. 2005, ApJ, 619, 12

Suchyta, E., Huff, E. M., Aleksić, J., et al. 2016, MNRAS, 457, 786

Tilvi, V., Pirzkal, N., Malhotra, S., et al. 2016, ApJ, 827, 14

Tilvi, V., Rhoads, J. E., Hibon, P., et al. 2010, ApJ, 721, 1853

Valdes, F., Gruendl, R. & DES Project 2014, in ASP Conf. Ser. 485, Astronomical Data Analysis Software and Systems XXIII, ed. N. Manset & P. Forshay (San Francisco, CA: ASP), 379

Willott, C. J., Carilli, C. L., Wagg, J., & Wang, R. 2015, ApJ, 807, 180

Zheng, Z. Y., Malhotra, S., Rhoads, J. E., et al. 2016, ApJS, 226, 23